crystals

MDPI

Article

Properties and Potential Application of Lead-Free ($BaZr_{0.2}Ti_{0.8}O_3$) and Lead-Based ($PbZr_{0.52}Ti_{0.48}O_3$) Flexible Thick Films

Jelena Bobić [1,*], Nikola Ilić [2], Željko Despotović [3], Adis Džunuzović [1], Robertas Grigalaitis [4], Ivan Stijepović [5], Biljana Stojanović [6] and Mirjana Vijatović Petrović [1]

[1] Department of Materials Science, Institute for Multidisciplinary Research, University of Belgrade, 11030 Belgrade, Serbia; adisdzunuz@imsi.rs (A.D.); mira@imsi.rs (M.V.P.)
[2] Department of Atomic Physics, Vinca Institute of Nuclear Sciences, National Institute of the Republic of Serbia, University of Belgrade, 11001 Belgrade, Serbia; nikola.ilic@vin.bg.ac.rs
[3] Mihajlo Pupin Institute, University of Belgrade, 11060 Belgrade, Serbia; zeljko.despotovic@pupin.rs
[4] Faculty of Physics, Vilnius University, LT-01513 Vilnius, Lithuania; robertas.grigalaitis@ff.vu.lt
[5] Department of Materials Engineering, Faculty of Technology, University of Novi Sad, 21000 Novi Sad, Serbia
[6] Academy of Engineering Sciences of Serbia, 11000 Belgrade, Serbia; bstojanovic80@yahoo.com
* Correspondence: jelena@imsi.rs; Tel.: +381-11-2085-039

Abstract: For the last several decades, energy harvesters based on piezoelectricity from mechanical vibration have emerged as very promising devices that are being explored extensively for their functionality in energy technologies. In this paper, a series of flexible lead-free $BaZr_{0.2}Ti_{0.8}O_3$ (BZT)/PVDF and lead-based $PbZr_{0.52}Ti_{0.48}O_3$ (PZT)/PVDF piezocomposites with variable filler content up to 50 vol% were prepared by a hot pressing method. The structure and morphology of the BZT and PZT powders, as well as the distribution of the piezo-active filler in the obtained flexible films were characterized by XRD and SEM analysis. In addition, the remnant polarization (P_r) and leakage current were also investigated to evaluate the breakdown strength in both types of flexible films. The calculations of storage energies and output voltage obtained for the investigated materials revealed an increasing trend with an increasing amount of BZT and PZT active phases. The maximum storage energy of 0.42 J/cm^3 (and energy efficiency of 40.7 %) was obtained for the PZT–PVDF (40–60) films, while the maximum output voltage of about 10 V (~10 μA) was obtained for the PZT–PVDF (50–50) flexible film. In addition, a comparison between the properties of the lead-based and lead-free flexible films, as well as the potential use of these films as energy storage and energy harvesting systems were analyzed.

Keywords: flexible films; ferroelectrics; dielectric properties; energy harvesting; energy storage

Citation: Bobić, J.; Ilić, N.; Despotović, Ž.; Džunuzović, A.; Grigalaitis, R.; Stijepović, I.; Stojanović, B.; Vijatović Petrović, M. Properties and Potential Application of Lead-Free ($BaZr_{0.2}Ti_{0.8}O_3$) and Lead-Based ($PbZr_{0.52}Ti_{0.48}O_3$) Flexible Thick Films. *Crystals* **2023**, *13*, 1178. https://doi.org/10.3390/cryst13081178

Academic Editor: Artem Pronin

Received: 6 July 2023
Revised: 24 July 2023
Accepted: 26 July 2023
Published: 28 July 2023

1. Introduction

Various alternative renewable sources, such as solar, wind, and thermal energy and mechanical vibrations, are available for energy generation. For the last several decades, energy harvesters based on piezoelectricity from mechanical vibration have been explored extensively for their functionality in energy technologies [1,2]. In the case of low power electronic devices, power utilization generally lies in the mW or μW range. Furthermore, the greater part of these applications involves a device that has the capacity to work both indoors and outdoors in such a manner that it does not possess a substantial dependence on climate conditions. Energy harvesting is a promising field that enables IoT (Internet of Things) devices to generate electrical energy by absorbing energy from the environment. The IoT manages a large infrastructure of web-enabled smart devices, small devices that use embedded systems, such as processors, sensors, and communication hardware, to collect, send, and elaborate on data acquired from their environment [3–5]. Ultra-low-power

consumption (up to tens of micro-amps per preamplifier) is a very important requirement in order to operate devices with small energy sources.

Compared to flexible electronics built on non-stretchable materials, stretchable materials withstand a greater amount of strain, thus making them more suitable for application scenarios with large bending and twisting requirements [6–8]. To fabricate a flexible piezoelectric energy harvester (FPEHs) that operates under various conditions, ceramic particles were blended with a polymer to form composite films (CFs). Polyvinylidene (PVDF) was chosen as an appropriate polymer matrix owing to its excellent stretchability and high flexibility [9–12].

Lead zirconate titanate (PZT)-based piezoelectric generators are commercially available and widely employed in the range of 0–200 °C [13,14]. It is well known that at the morphotropic phase boundary region, PZT's (Zr/Ti = 58/42) composition provides the best dielectric, ferroelectric, piezoelectric, and pyroelectric properties [15]. However, the family of lead-based materials is facing challenges due to its environmental incompatibility due to the toxicity of lead. The presence of lead implies danger during the manufacture, use, and disposal of these materials. Therefore, there is a growing need for new lead-free materials for various applications. Lead-free solid solutions of $BaTiO_3$ and $BaZrO_3$ ($Ba(Zr_xTi_{1-x})O_3$, abbreviated as BZT) are among the most important compositions for dielectrics in multilayer ceramic capacitors [16]. BZT ceramics have attracted immense attention due to their high dielectric constant, low dielectric loss, and large tunability because the substitution of Zr^{4+} for Ti^{4+} ions has a beneficial effect on the stability of the system [17,18]. Even though a large number of studies have evaluated BZT ceramics, a rather limited number of studies have incorporated BZT flexible composite films. On the other hand, there are many reports on other more complex lead-free systems, such as $BaZrTiO_3$–$BaCaTiO_3$ and $(Bi_{0.5}Na_{0.5})TiO_3$–$BaTiO_3$, which have been shown to be the most promising materials with great piezoelectric performance [19–24]. Because of the aforementioned lack of study of composite films, we examined the simple-structured BZT and PZT composite films with a potential for energy storage and energy harvesting usage that can be good alternatives to the complex lead-free systems.

In the present work, a solid-state synthesis method was used in order to obtain the appropriate $BaZr_{0.2}Ti_{0.8}O_3$ active phase. Flexible BZT/PVDF films were fabricated by the hot-pressing method. In addition to the BZT-based films, PZT-based flexible films were also prepared using PZT powders obtained by an auto-combustion method. The conditions for preparing both types of films with homogeneous distribution of the piezo-active filler were carefully optimized. The motivation behind choosing these two particular compositions of BZT and PZT as active phases in flexible films is to examine the pros and cons of using these simple-structured materials, in terms of their functionality, for energy harvesting and energy storage.

2. Methods

2.1. Experimental Procedure

Powder of $BaZr_{0.2}Ti_{0.8}O_3$ was synthesized by a solid-state reaction route. The stoichiometric amounts of appropriate oxides TiO_2 (99.9%, Degussa), ZrO_2 (99.9 %, Aldrich), and $BaCO_3$ (99.0 %, Merck) were ball-milled in ethanol for 48 h. The dried precursor mixture was calcined at 1370 °C for 4 h and ground thoroughly in an agate mortar.

The PZT powder was synthesized by an auto-combustion method. Appropriate analytical-grade metal nitrates (lead nitrate ($Pb(NO_3)_2$), zirconium (IV) oxynitrate hydrate ($ZrO(NO_3)_2{\cdot}H_2O$), titanium isopropoxide ($Ti(OCH(CH_3)_2)_4$)), and citric acid ($C_6H_8O_7{\cdot}H_2O$) were used as the starting materials. A detailed powder preparation method was reported in Ref. [25]. After the auto-combustion synthesis and calcination of the PZT precursor powder at 800 °C for 4 h, pure PZT powder was obtained.

Commercial PVDF powder (Alfa Aesar), which is mainly composed of α-phase, and the BZT powders were mixed in three different ratios, namely, 30, 40, and 50 vol% of the BZT powders. The samples were named according to the amount of as-prepared filler:

BZT–PVDF(30–70); BZT–PVDF(40–60), and BZT–PVDF(50–50). The same procedure and volume ratio between the active phase powder and polymer matrix was used for the samples with PZT powder. To obtain high-performance dielectric composites, it is very important to disperse ceramic nanoparticles into the polymer matrix homogeneously. Thus, the powder of the active phase was mixed with the PVDF powder using an ultrasonic probe in the isopropanol medium for 15 min for better homogenization. After drying, the powder mixture was placed between two Kapton sheets and hot-pressed using a custom-built set-up. The hot-pressing procedure consisted of heating up the powder to 190 °C for 5 min while applying pressure of 5 MPa, followed by natural cooling. Figure 1a shows the obtained flexible film in the shape of a disk with diameter around 3–4 cm that possesses good flexibility. The thicknesses of the BZT films with 30, 40, and 50 vol% were 60 µm, 110 µm, and 250 µm, respectively. Thinner films were obtained for the PZT powders, and the values are 45 µm, 60 µm, and 90 µm for 30, 40, and 50 vol% of the active phase, respectively. The thicknesses of the samples were measured by a digital comparator.

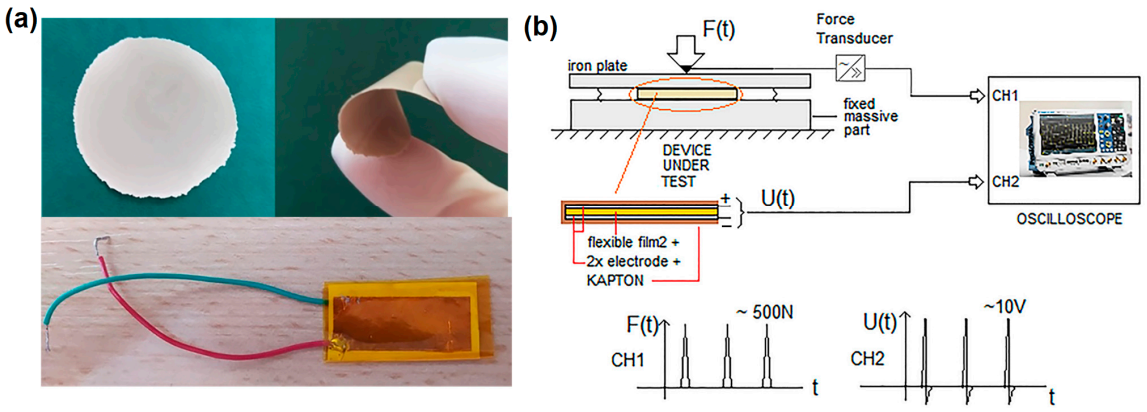

Figure 1. (**a**) BZT–PVDF film obtained by hot-pressing method; below that is a picture of the assembled component for testing. (**b**) Scheme of testing set-up.

2.2. Characterization of Powders and Composite Films

The structure of the synthesized BZT and PZT powders was investigated using XRD measurements (Rigaku MiniFlex 600 instrument, Rigaku, Cedar Park, Texas, USA). The morphology of the powders and composite films was investigated by a Tescan VEGA TS 5130MM microscope and FESEM (Tescan Mira 3 XMU, Tescan, Brno, Czech Republic). The vibrational spectrum obtained through Fourier transform infrared spectroscopy (FTIR, PerkinElmer Spectrum Two™, PerkinElmer, Inc, Waltham, Massachusetts, USA) is useful for the identification and determination of the amount of the electroactive phases (β and/or γ). The analyses were carried out in attenuated total reflectance (ATR) mode in a wavenumber of 4000–400 cm^{-1}. In order to estimate the relative fraction of the electroactive phases (F_{EA}), Equation (1) was used:

$$F_{EA} = \frac{I_{EA}}{1.26\, I_{\alpha} + I_{EA}} \times 100 \quad (1)$$

where I_{EA} is the absorbance of the band at about 840 cm^{-1} that can be assigned to the β and/or γ phase and I_{α} is the absorbance of a characteristic band of the α phase [26,27]. The ratio between the absorption coefficients at the respective wavenumbers is 1.26. In the case that the β and γ phases coexist simultaneously in the film, it is possible to separate these two contributions (F_{β}) and (F_{γ}) by taking the peak-to-valley height ratio between the two peaks around 1275 and 1234 cm^{-1}, as suggested by X. Cai et al. [26].

For the electrical characterization, the flexible films were cut into pieces of 2.5 × 1 cm and covered with silver electrodes with an area of 1.5 cm^2 by applying the silver paint (Sigma Aldrich). The dielectric permittivity measurements were carried out using an LCR meter (model 4284A, Hewlett-Packard, Palo Alto, California, USA) in a temperature

range of 130 to 420 K and a frequency range of 100 Hz to 1 MHz. A precision multiferroic test system with a high-voltage interface (Radiant Technologies, Inc., Albuquerque, New Mexico, USA) up to 4000 V was employed for the ferroelectric characterization and leakage current measurements at room temperature. The polarization curves were measured at different external electric fields at a frequency of 100 Hz.

2.3. Preparation of Films for Testing

Before energy harvesting testing, the films needed to be poled in order to align the domains of the active phase into one direction to obtain good functional material [28]. Electrical poling of the samples was performed between the parallel metal plates in a silicon bath. The poling procedure was performed in an electrical field of 50 kV/cm at a temperature of 135 °C for 40 min, after which, the samples were cooled down to 50 °C in an electric field off.

After poling, the samples were wired with Cu wires in order to enable a connection with the external circuit. Furthermore, the films were wrapped in insulation Kapton tape (polyimide film), which is flexible and provides protection to the testing modulus from mechanical strikes (Figure 1a below). Energy harvesting testing was carried out using a quartz impulse hammer with an IEPE output modal (KISTLER Instrument Corporation, Amherst, NY, USA) by applying a force impact of 500 N. The testing set-up scheme is presented in Figure 1b.

3. Results and Discussion

Flexible Films Obtained from Prepared Solid-State BZT Powders

The XRD pattern reported in Figure 2a shows that the single-phase BZT powder was obtained after calcination at 1370 °C for 4 h. Using Rietveld refinement of the XRD data with MAUD software (version 2.33) [29], the coexistence of 47 % cubic (*Fm3m*) and 53 % tetragonal phase (*P4/mmm*) was found. The XRD diffractogram of the morphotropic PZT52/48 powder calcinated at 800 °C for 4 h is shown in Figure 2b. The coexistence of 80 % of the tetragonal (*P4mm*) and 20 % of monoclinic phase (*Cm*) was found. The earliest investigations of the $Pb(Zr_{1-x}Ti_x)O_3$ properties near MPB showed that the highest values of the dielectric constants are on the tetragonal side, while the highest piezoelectric constants are on the monoclinic/rhombohedral side of the transition [30]. In our case, the tetragonal phase prevails, which implies good dielectric properties of the obtained films.

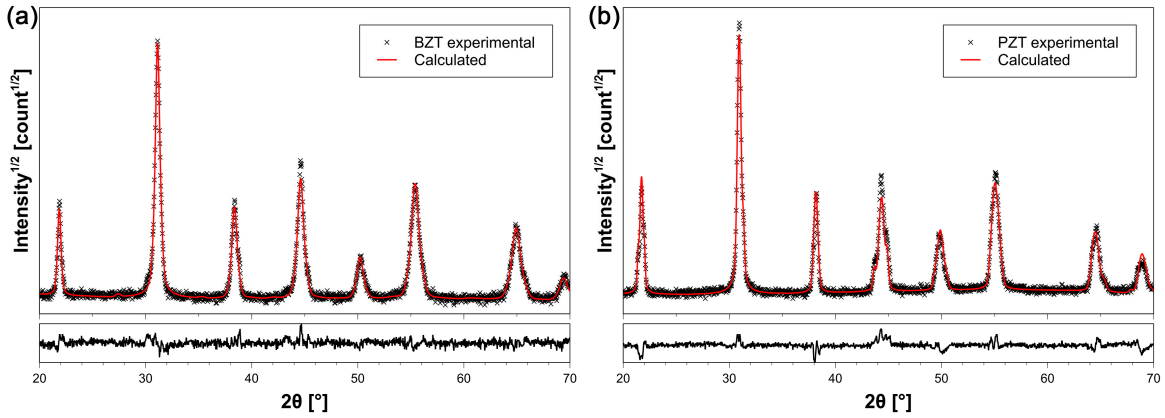

Figure 2. X-ray diffractograms of (**a**) BZT powders calcinated at 1370 °C for 4 h and (**b**) PZT powders calcinated at 800 °C for 4 h.

The SEM images of cross-sections of the BZT–PVDF and PZT–PVDF flexible films demonstrating different filler content are presented in Figure 3. The volume ratio was chosen in order to fulfill the requirements for the characteristics on one side and the flexibility of the films on the other. Very good flexibility of the films was achieved through the addition of 30 and 40 vol% of the active filler phase. By increasing the volume of the

ceramic filler in the film, the flexibility notably decreased, but still retained in a certain level with the addition of 50 vol% of filler. However, a thoroughly homogeneous distribution of the piezo-active filler was confirmed by SEM in the BZT–PVDF samples. Contrary to that, in the PZT–PVDF films, the distribution of the active phase filler in the polymer matrix was not so homogeneous. The PZT powder is prone to agglomeration during auto-combustion synthesis, and it is very difficult to achieve uniform dispersion of the powder in the matrix [31].

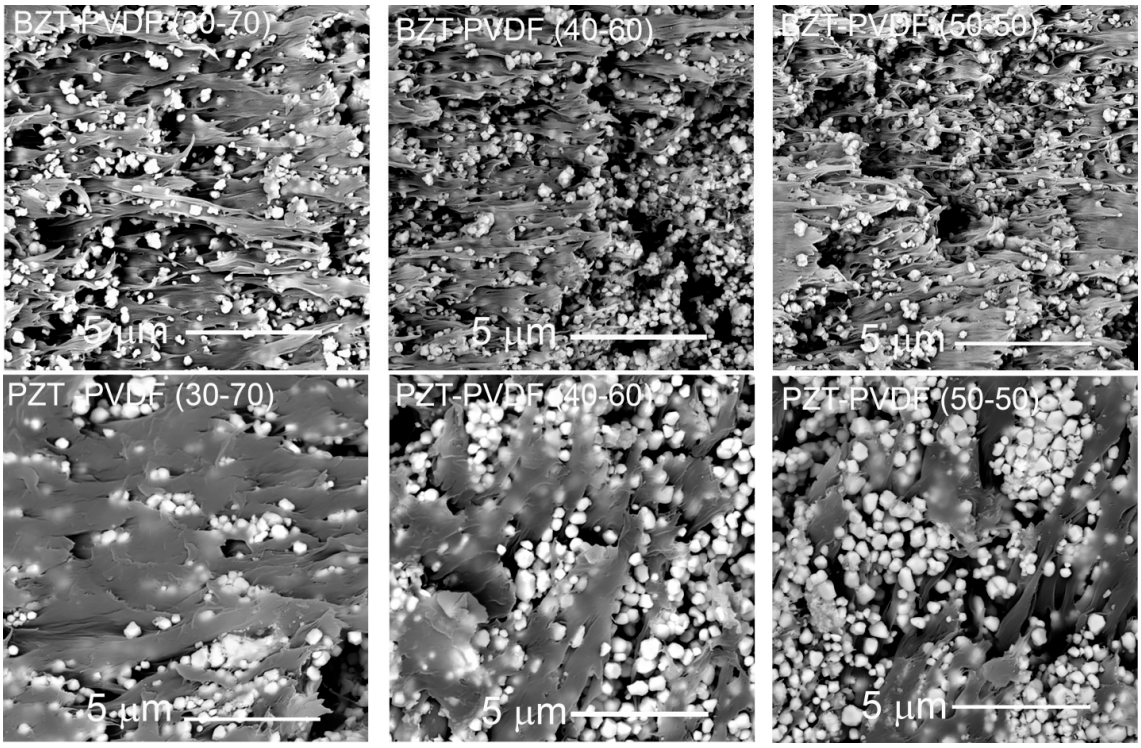

Figure 3. The SEM images of cross-sections of different compositions of BZT–PVDF and PZT–PVDF films.

The FTIR spectra of pristine PVDF and all the composite films were used to study the interaction of the filler and the polymer and the amount of the electroactive phase of PVDF in each sample (Figure 4). There are several different polymorphs in the PVDF phase, out of which α, β, and γ configurations are the most representative [25,27]. The relative quantity of each depends on the thermal, mechanical, and electrical processing conditions used to produce the PVDF film. The α-phase is not electroactive, while the other two are, with β possessing larger polarity than the γ-phase [3]. Among all the polymorphs in the PDVF, the β-phase shows the highest net dipole moment and, as a result, outstanding piezo- and pyroelectric properties. Thus, there is an interest in increasing its proportion within the other phases to maximize the electrical output of PVDF-based piezoelectric generators [32].

The characteristic absorption bands of the non-active α-phase can be observed around at 1423, 1383, 1209, 1149, 975, 854, 795, 763, 614, 532, 489, and 410 cm^{-1}, and those of the β-phase at 1431, 1275, 1072, and 840 cm^{-1}. The γ- and β-phase show a similar number of bands, most of which appear at a similar wavenumber due to the similar polymer chain conformation [10,12]. However, it was found that the bands around 763 and/or 614, 1275, and 1234 cm^{-1} can be consistently used to differentiate and identify the α-, β-, and γ-phases, respectively. Equation 1 was used to calculate the PVDF phases in all the composites film and the results are reported in Table 1. Which phase will be formed in PVDF composite films depends on many factors, such as the preparation method of the composite films (viscosity of the solution, polarity of the solvent, and the induced thermal

energy), particle size, and distribution and morphology of the filler, as well as the amount of the filler content [10,22,33].

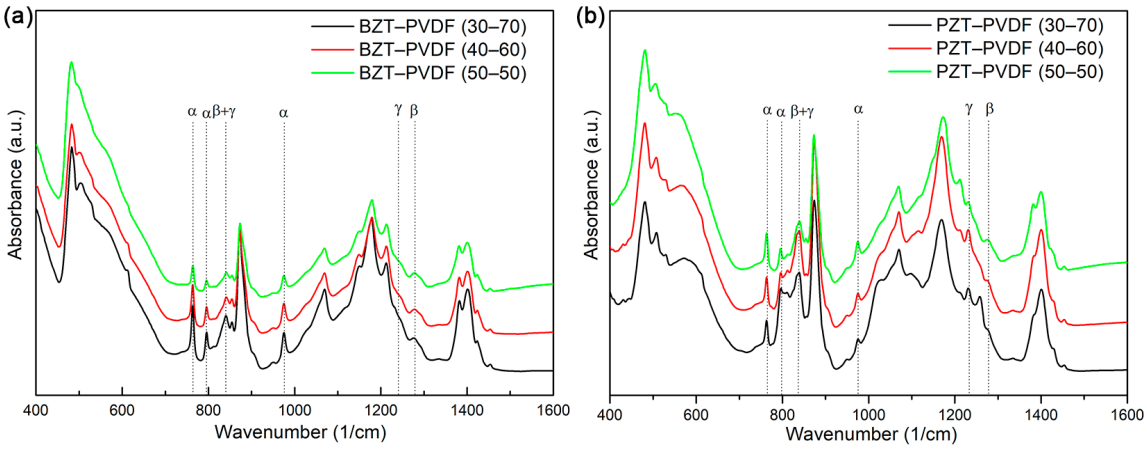

Figure 4. FTIR spectra of all flexible (**a**) BZT-based and (**b**) PZT-based films.

Table 1. Amounts of α and electroactive phases β- and γ-phases in all composite flexible films.

Samples	$\%F_\alpha$	$\%F_\beta$	$\%F_\gamma$	$\%F_{EA}$
PVDF	46	4	50	54
BZT–PVDF (30–70)	58	42	/	42
BZT–PVDF (40–60)	61	39	/	39
BZT–PVDF (50–50)	55	45	/	45
PZT–PVDF (30–70)	36	/	63	63
PZT–PVDF (40–60)	36	/	63	63
PZT–PVDF (50–50)	47	22	31	53

Pristine PVDF (which is mainly composed of α-phase) crystallized mainly in the γ-phase (50 %) and a very low amount in the β-phase (4 %) during preparation of the films. After preparing of the flexible films by different methods (such as the Langmuir–Blodgett method, spin coating, and solvent casting) many authors further processed their films by hot-pressing in order to enhance the polar phase in PVDF [34–36]. On the other hand, the generation of the β-phase directly from the melt is very much in demand and requires extreme conditions. For instance, Scheinbeim et al. [37] applied very high pressure in the range of 200 to 800 MPa, confirming the formation of a purely β-phase by applying the highest pressure of 800 MPa. We used the hot-pressing method (with a pressure of 5 MPa) to avoid solvents usually used for the dissolution of PVDF, which made the process of preparation of our films more facile and cost-effective.

The added BZT particles induce the PVDF polymer to crystallize in a more polar β-phase. The amount of the electroactive β-phase in the BZT–PVDF-based films does not vary much when increasing the ceramic filler amount, but the highest amount of electroactive phases (around 45 %) was found in the composition of BZT–PVDF (50–50).

On the other hand, PZT particles induce the formation of more γ-phase (63 %), especially in the PZT–PVDF (30–70) and PZT–PVDF (40–60) films. The appearance of the peak at 1275 cm^{-1}, the main characteristic of the β-phase, and the characteristic peaks of the α- and γ-phases can be seen only in the PZT–PVDF (50–50) sample. The nucleation of the ferroelectric β-phase should generally be strongly induced by the interaction between the surface charges of the filler with the dipole of the polymer. As already mentioned, the PZT particles were prone to agglomeration, thus the ionic dipole interactions became weaker and the critical number of centers for the nucleation of the β-phase did not even

exist in the PZT–PVDF (30–70) and PZT–PVDF (40–60) films. However, with the increase of the active filler up to 50 %, the β-phase appeared instead of the γ-phase. With the increase of the filler concentration, the interactions between the filler and polymer matrix became more pronounced and, as a result, the formation of the β-phase was enhanced [38]. The total amount of the electroactive phase (% F_{EA}) was higher in the PZT-based films in comparison with the BZT-based ones; however, the contribution of more the desirable and more electroactive β-phase was higher in the BZT–PVDF films.

The dielectric constant and dielectric loss (tanδ) are very important parameters for ferroelectrics, as the dielectric constant represents the charge-holding capacity and tanδ denotes the power loss in each cycle of measurement [39]. Figure 5 shows the temperature dependence of ε′ and the tan δ of the neat PVDF, BZT–PVDF (30–70), and PZT–PVDF (30–70) films at a temperature range from 130 K to 420 K and a frequency range from 20 Hz to 1 MHz.

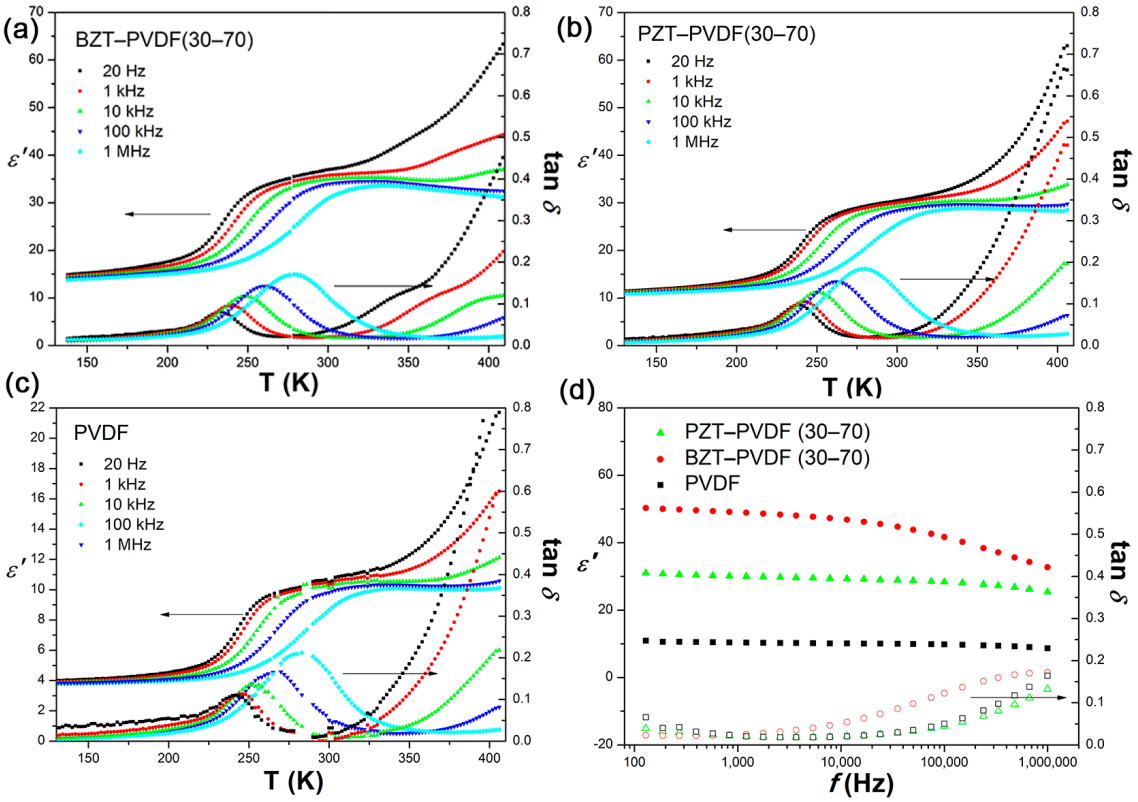

Figure 5. Temperature dependence of the dielectric constant and tan δ of (**a**) neat PVDF, (**b**) BZT–PVDF (30–70), and (**c**) PZT–PVDF (30–70) at different frequencies; (**d**) frequency dependence of dielectric constant and tan δ at room temperature.

The dielectric properties of the composites are influenced by different factors, such as the amount and morphology of the filler, dispersion, volume fraction of the filler, and the interactions between the two phases [40]. For the neat PVDF film, as well as for both types of composites, the dielectric constant was almost frequency-independent in the low temperature region (up to 200 K). Above this temperature and up to 350 K, the dispersed regions appear. Its main feature is the shifting of the maximum of the dielectric loss to higher temperatures as the frequency increase. This behavior generally implies that the dipolar system has a broad distribution of relaxation time [41]. In the investigated composites, this dispersion can be attributed to the relaxation of frozen C–F dipoles in the amorphous region of PVDF. When the freezing temperature (T_f) is reached, these C–F dipoles receive enough energy and start to move. This relaxation was seen in the pure PVDF, as well as in the BZT–PVDF and PZT–PVDF films, and it is attributed to the so-called β-relaxation [25,42]. The second dispersion above 350 K manifested through the

strong increase of the dielectric permittivity, especially at lower frequencies, which most likely originates from the expressed conductivity. Some authors suggest that it can be also attributed to the mobility of the crystalline part of the polymer chains, while others think that the main reason is interfacial polarization of different types: polarization due to the accumulation of space charge in the interface region between the PVDF matrix and filler particles and/or at the boundaries between the crystalline and amorphous PVDF phases [43]. Both dispersions were more expressed in the BZT–PVDF films in comparison to the PZT–PVDF films.

The frequency dependence of the dielectric properties of the BZT/PZT–PVDF (30–70) composites and the neat PVDF film at room temperature is given in Figure 5d. In the whole frequency range, a higher dielectric constant was observed in the BZT-based films ($\varepsilon' \approx 42$) than in the PZT-based one ($\varepsilon' \approx 30$). It was also found that both composites had higher permittivity in contrast to their polymer host matrix ($\varepsilon' \approx 10$) [23]. The enhancement of the dielectric constant of the composite films in comparison to the neat PVDF film can be ascribed to the dipole polarization and interfacial polarization induced by the BZT/PZT fillers having three or more times higher dielectric constant [44].

As it can be seen from Figure 5, compared to neat PVDF, the value of the dielectric losses of the composite films remained almost the same in the whole temperature range at lower frequencies. The loss curve maintained smoothness in the frequency range from 100 Hz to 1 kHz and then a sharp increase was noted around 10 kHz, which is a typical feature of the glass transition relaxation of the PVDF matrix. In this frequency range, the dielectric losses of the BZT–PVDF film were the highest, with the probable reason being that the amorphous phase of the PVDF in that film was at its highest in this frequency range in comparison to other two.

The polarization versus electric field hysteresis loops (P–E loops) were recorded at 10 Hz at room temperature (Figure 6). The highest breakdown field that BZT–PVDF (30–70) can endure is 135 kV/cm; therefore, all the polymer composites are displayed for that field (Figure 6a,b). However, none of the flexible films can sustain a high enough field to demonstrate saturated hysteresis loops probably because of its polycrystalline nature. Instead, the hysteresis loops of all the composite films are symmetrical, well-defined, and nonlinear. The ferroelectric measurements of the neat PVDF confirmed dielectric behavior with completely linear hysteresis loops up to 135 kV/cm. The hysteresis loops of the composite films show that the polarization response was significantly influenced by the incorporation of the filler particles within the PVDF matrix, showing an enhancement in the remnant polarization and coercive field values with the higher content of the ferroelectric active phase. On the other hand, the highest values of polarization (P_R) at zero fields and the lowest coercive field (E_C) were obtained for both types of compositions with 50 vol% of the filler particles. The samples that reached the highest breakdown field were BZT–PVDF (40–60) at a field of 220 kV/cm and PZT–PVDF (40–60) at a field of 390 kV/cm; these hysteresis loops are presented at Figure 6c.

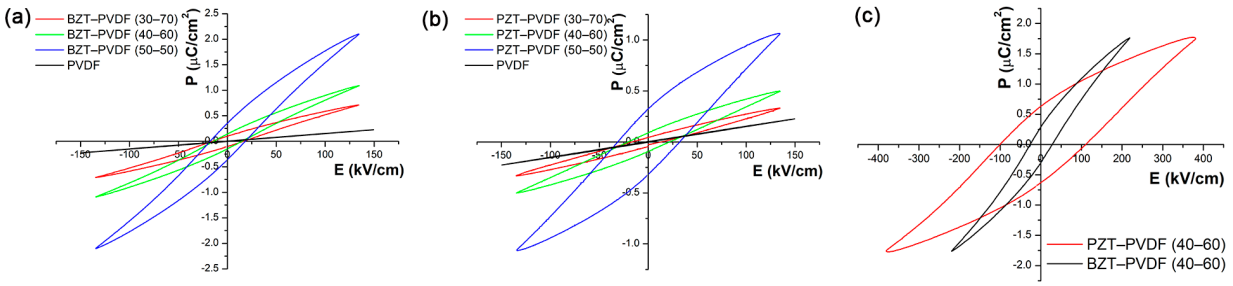

Figure 6. Ferroelectric hysteresis loops of all flexible films: (**a**) BZT–PVDF films, (**b**) PZT–PVDF films, and (**c**) BZT–PVDF (40–60) and PZT–PVDF (40–60) films exhibiting the highest measured breakdown fields.

The current density (J) was measured as a function of the static electric field (E) in order to study the conductivity mechanism in the material (Figure 7). As in the case of the ferroelectric measurements, the leakage current density did not reach saturation. In a low-field region, the leakage current was low, suggesting an ohmic (linear) conduction behavior. However, it increased rapidly when increasing the applied electric field. This increase can most likely be attributed to the co-existence of both ohmic and space charge limited-conduction mechanism [45]. Bearing in mind that the leakage current is related to the electric conductivity, it implies somewhat higher electrical conductivity of the PZT–PVDF composite films in comparison to BZT–PVDF.

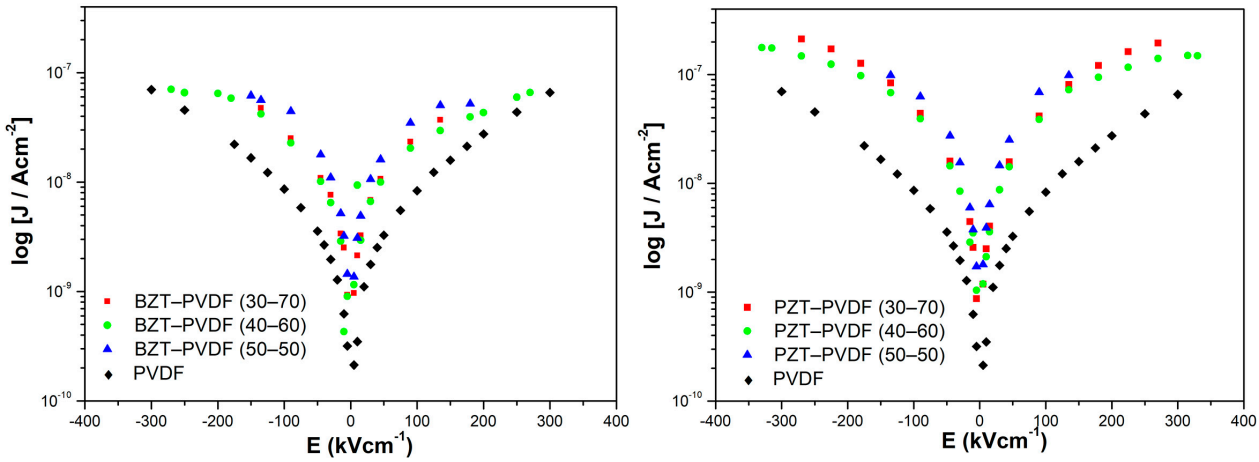

Figure 7. Current densities as a function of static electric field.

However, in both types of composites, the electric conductivity was not significantly influenced by the amount of the active phase.

To design a proper dielectric material with high recoverable energy-storage density and high efficiency (small energy loss) for practical applications, at least three requirements have to be satisfied simultaneously: a high electric breakdown field, large saturated polarization, and small remnant polarization [46]. For researchers to investigate the potential for energy storage of composite films, the hysteresis results are presented in the form of electric displacement–electric field loops at an applied field of 135 kV/cm (Figure 8). The derived values of the energy density presented in Table 2 show that the energy density (J_{tot}) became higher with the amount of active phase and it reached a value of 0.15 J/cm^3 for BZT–PVDF (50–50) and 0.09 J/cm^3 for PZT–PVDF (50–50). Also bearing in mind that the field of 135 kV/cm is quite low, the values obtained for the energy density are, accordingly, low. The samples that reached the highest breakdown field were BZT–PVDF (40–60) (220 kV/cm^3) and PZT–PVDF (40–60) (390 kV/cm^3), and the energy densities at these higher fields were 0.21 J/cm^3 and 0.42 J/cm^3, respectively. The breakdown strength diminished with the increasing filler content above 40 wt%, most likely because the amount of defects, such as micro-cracks and voids, increased with the concentration of filler nanoparticles.

It is known that the energy-storage density in bulk antiferroelectric ceramics is usually less than 1 J/cm^3 due to the lower breakdown field (below 60 kV/cm) caused by the interior defects in the pores during the sintering process [3]. In the case of polymer-based composite films with different fillers, the energy densities were in the range of 2–7 J/cm^3 measured at very high electric fields of 1000–4000 kV/cm [3,19,47–50]. The literature data have shown that the results of energy storage can vary significantly due to the synthesis methods of the active phase, the amount of active filler, different preparation procedures of the films (tape casting on a substrate, casting in a petri dish), synthesis methods of the active phase, the thickness and dimensions of the films, the amount of active filler, the presence of coupling agents (dopamine, APTES, DDTES, etc.), the number of layers (type of sandwich structure), etc.

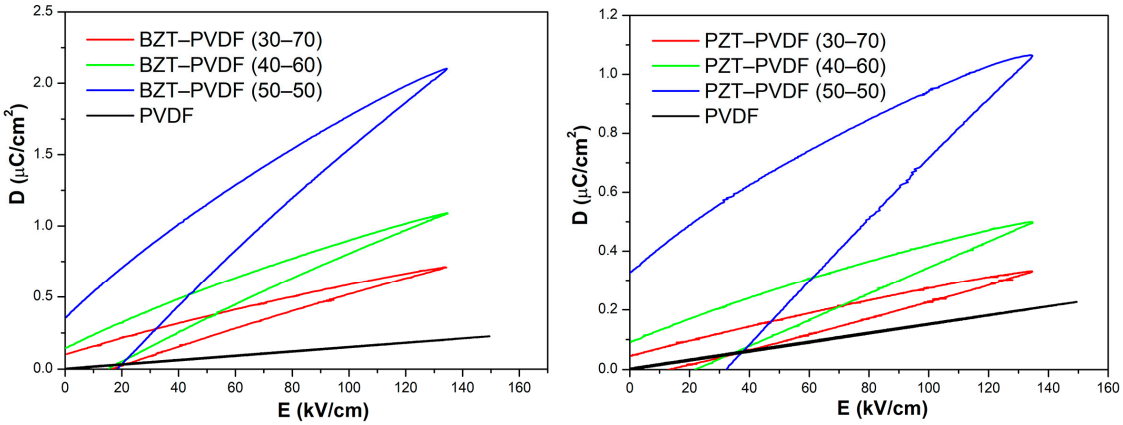

Figure 8. Electrical displacement vs. electric field loops for investigated flexible composite films.

Table 2. Energy loss density (J_{loss}), the energy-storage density (J), total energy density (J_{tot}), and energy density efficiency (η) for both composites at 135 kV/cm.

Samples	J_{loss} (J/cm^3)	J (J/cm^3)	J_{tot} (J/cm^3)	η (%)
PVDF	0.001	0.06	0.061	98.4
BZT–PVDF (30–70)	0.0148	0.0371	0.0519	71.5
BZT–PVDF (40–60)	0.0214	0.0572	0.0786	72.7
BZT–PVDF (50-50)	0.0502	0.103	0.1532	67.2
PZT–PVDF (30–70)	0.0078	0.0176	0.0254	69.2
PZT–PVDF (40–60)	0.0147	0.0245	0.0392	62.5
PZT–PVDF (50–50)	0.0465	0.0411	0.0876	46.9

Generally, it was found that the composites had increased permittivity in contrast to their polymer host matrix, but in some cases, they also displayed decreased breakdown strength and raised energy loss. Large differences in the relative permittivity between the active phase particles and polymer matrix leads to an inhomogeneous electric field distribution, since electric fields tend to concentrate in the interfacial region (around the filler particles) [51]. This occurred in the investigated composite films, in which the neat PVDF film endured the maximum electric field (that our voltage source allows—4000 V), while in the composite films, the breakdown process occurred at lower fields. When an electric field is applied, a local electric field is formed in the interface region, increasing the possibility of the electrical breakdown. As the concentration of the filler particles increases, the direct contact between the particles is more pronounced which can also lead to the decrease of breakdown strength. Additionally, the agglomeration and phase separation from the matrix due to the high surface energy of the dielectric ceramic result in a high defect density in the composite, which leads to a breakdown.

Nevertheless, the obtained results point to the potential of the investigated materials for energy-storage applications. Besides their high energy density, for the practical application in energy-storage devices, it is important that the material possesses high efficiency. The percentage of energy-storage efficiency (η) is calculated by dividing the energy-storage density (J) by the total energy density (J_{tot}) and multiplying by 100. The energy density efficiencies obtained from the *D*–*E* loops for the investigated materials are presented in Table 2 and show a decreasing trend with the increasing amount of the BZT/PZT active phase (from 72.7 down to 47.1%). Even though these are relatively low values of energy-storage densities, they are comparable with values of complex flexible films, such as $0.5(Ba_{0.7}Ca_{0.3})TiO_3$-$0.5Ba(Zr_{0.2}Ti_{0.8})O_3$/PVDF obtained by a solution casting method, where the maximum breakdown strength is 1340 kV/cm and the corresponding energy-storage density is 0.72 J/cm^3 obtained from the filler content of 10 wt% [21]. Dash

et al. found that the energy-storage density (0.73 J/cm^3 at an electric field of 750 kV/cm) of the composite films with 15 wt% of hydroxylated BZT–BCT particles is much higher than those of the unhydroxylated BZT–BCT sample, pure PVDF–HFP copolymer, and their composites [20]. An extremely high energy-storage density of the dopamine-modified BZT nanofibers and PVDF composite of 13.0 J/cm^3 was obtained with 5 vol% BZT filler at 5219 kV/cm [51]. An energy-storage density of 6.3 J/cm^3 was obtained at 3800 kV/cm for 2.5 vol% PVP-modified BZT nanofibers [50].

Obviously, an effective approach to overcome the low energy density of simple-structured BZT and PZT composite films is the addition of the surface modifier of the filler particles with a variety of organic modifiers in order to enhance the dispersion of the nanofillers in the polymer matrix and to enhance the breakdown strength. Another method is the preparation of sandwich/multi-layer-structured nanocomposites, which already have shown their potential through the improved breakdown strength and high energy density [52,53]; this will be the main topic of future research.

The voltage generation of the polymer/ceramic composites BZT and PZT/PVDF while applying the impact force of 500 N are presented in Figure 9. The output voltage of the BZT/PVDF composite film was 3 V, 6 V, and 7 V for BZT–PVDF (30–70), BZT–PVDF (40–60), and BZT–PVDF (50–50), respectively. For the same impact force, the output voltage of the PZT/PVDF films was 6 V, 8 V, and 10 V for compositions PZT–PVDF (30–70), PZT–PVDF (40–60), and PZT–PVDF (50–50), respectively. The PZT-based composite films had slightly higher output voltage than that achieved in the BZT-based films. In both types of films, with the increase of the BZT/PZT nanoparticles content, the output voltage increased.

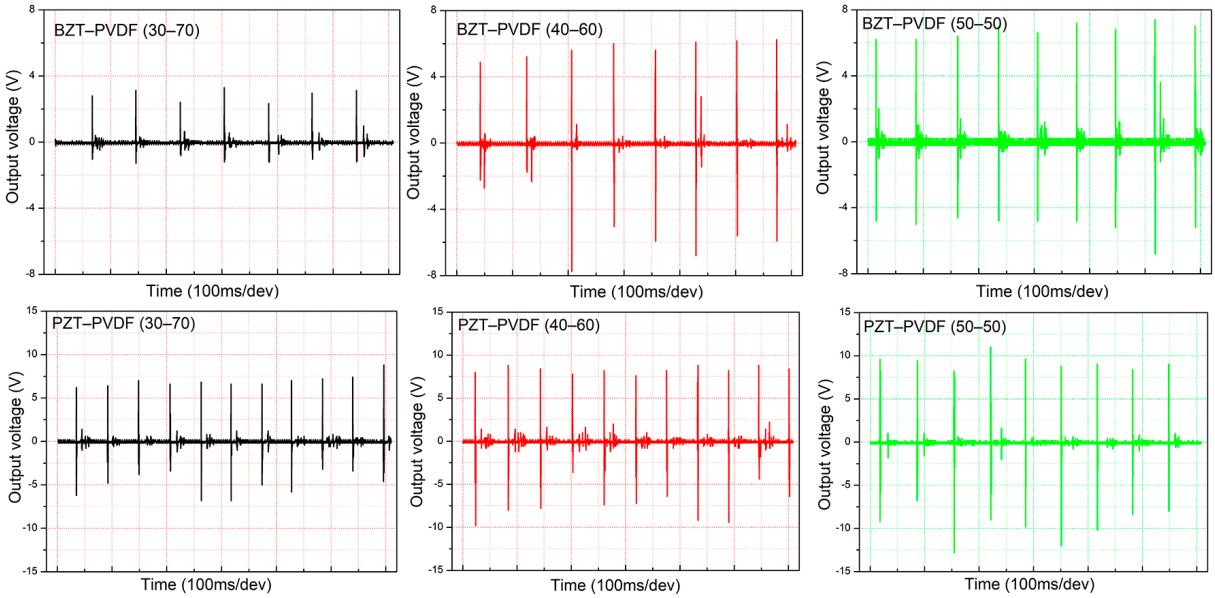

Figure 9. Oscilloscopic records of the voltage output obtained by applying 500 N of the impact force for all the composite films.

The energy-harvesting performance was characterized by many authors in different composites systems (Table 3). Biomechanical foot-tapping of BCZT/PVDF-HFP achieved a maximum output voltage of 4.55 V [54], while the maximum open-circuit voltage of 8.11 V was obtained with 30 wt% content of the BZT–BCT/P(VDF–TrFE) polymer film [55]. Liu et al. found an excellent output performance of 40% content of the BZT–BCT flexible film, which produced an output voltage as high as 13.0 V under cyclic tapping under 6 N and 10 Hz [56]. Shin et al. found that the output voltage of the flexible piezoelectric energy harvesters based on the BT/PVDF composite film was 15.7 V when applying 500 N forces, while those of the FPEHs based on the BZT and Cu-BZT NPs/PVDF composite films were 16.3 and 17.4 V, respectively [19]. A PZT/PVDF piezoelectric nanogenerator produced an output voltage of 2 V by human motion [13].

Table 3. Literature overview of energy-harvesting performance in different composites systems.

Sample	Preparation Method	*F* (N)	*U* (V)	Ref.
BCZT/PVDF–HFP	Solution-casting technique	Foot-tapping	4.55	[54]
BZT–BCT/P(VDF–TrFE)	Spin-coating onto substrate	10 N	8.11	[55]
BZT–BCT/ P(VDF–TrFE)	Spin-coating onto substrate	6 N	13.0	[56]
BT/PVDF	Dropped onto a substrate	500 N	15.7	[19]
BZT/PVDF	Hot-pressing method	500 N	8.0	this work [25]
PZT/PVDF	Coated film on mica substrate	Body motion	2	[13]

Considering all the different conditions of energy harvesting testing and setups that are being used in the abovementioned studies, the output voltage of our FPEH was lower in comparison with some literature data of similar or more complex systems. However, it is high enough to be a potential candidate for some self-powered devices. The highest values of the output current in our samples were found for the PZT–PVDF (50–50) composition (~10 μA) and the maximum of the generated power was up to 100 μW. This power is enough for many sensing (humidity, temperature sensors) and computing jobs. Our research findings suggest that these simple heterostructures might be adequate to harvest electrical energy from the surroundings, but additional modification of the material will be needed for enhanced energy storage.

4. Conclusions

Single phases of lead-free ($BaZr_{0.2}Ti_{0.8}O_3$) and lead-based ($PbZr_{0.52}Ti_{0.48}O_3$) flexible composite thick films were successfully obtained by the hot-press method in different volume percentages xBZT/PZT–(1-x)PVDF, where x = 30, 40, 50. Quite homogeneous distribution of a piezo-active filler was confirmed by SEM in the BZT–PVDF samples, while the PZT–PVDF samples showed higher agglomeration of the PZT particles and, consequently, less homogeneous distribution of the active filler in the polymer matrix. The total amount of the electroactive phase (% F_{EA}) of PVDF was higher in the PZT-based films in comparison with the BZT-based ones, but the contribution of the more desirable β-phase was higher in the BZT–PVDF films. In both composite systems, the dielectric permittivities were increased in contrast to their polymer PVDF host matrix, but they also displayed decreased breakdown strength and raised energy loss. The difference in the relative permittivity of the PVDF matrix and filler, as well as the agglomeration and phase separation of both ceramics leads to low energy-storage densities values. The samples that reached the highest breakdown field were BZT–PVDF (40–60) (220 kV/cm) and PZT–PVDF (40–60) (390 kV/cm), and the corresponding energy densities at those fields were 0.21 J/cm^3 and 0.42 J/cm^3, respectively. The samples with the highest amount of active phase for both types of the films showed the largest output voltage (for PZT/PVDF (50–50) around 10 V that generates power up to 100 μW).

Author Contributions: Conceptualization, J.B and M.V.P.; methodology, R.G.; I.S. and Ž.D.; validation, J.B.; N.I.; Ž.D.; A.D.; R.G.; I.S.; B.S. and M.V.P.; formal analysis, J.B.; N.I.; Ž.D.; A.D.; and M.V.P.; investigation, J.B.; N.I.; A.D. and M.V.P.; writing—original draft preparation, J.B.; writing—review and editing, M.V.P., I.S. and N.I.; visualization, J.B.; supervision, M.V.P. and B.S.; All authors have read and agreed to the published version of the manuscript."

Funding: This research was founded by Ministry of Science, Technological Development and Innovation Republic of Serbia (Grant No.: 451-03-47/2023-01/200053, 451-03-47/2023-01/200134 and 451-03-47/2023-01/200103).

Data Availability Statement: The data presented in this study are available on request from the corresponding author.

Conflicts of Interest: The authors declare that they have no known competing financial interests or personal relationships that could have appeared to influence the work reported in this paper. The authors declare the following financial interests/personal relationships which may be considered as potential competing interests.

References

1. Maiwa, H. Piezoelectric energy harvesting. In *Piezoelectric Materials*; Ogawa, T., Ed.; Intech: Rijeka, Croatia, 2016. [CrossRef]
2. Guo, S.; Duan, X.; Xie, M.; Aw, K.C.; Xue, Q. Composites, fabrication and application of polyvinylidene fluoride for flexible electromechanical devices: A Review. *Micromachines* **2020**, *11*, 1076. [CrossRef]
3. Wang, Y.; Yao, M.; Ma, R.; Yuan, Q.; Yang, D.; Cui, B.; Ma, C.; Liu, M.; Hu, D. Design strategy of barium titanate/polyvinylidene fluoride-based nanocomposite films for high energy storage. *J. Mater. Chem. A* **2020**, *8*, 884–917. [CrossRef]
4. Nayak, B.; Mansingh, A.; Machwe, M.K. Dielectric studies of PZT-polymer composites. *J. Mater. Sci.* **1990**, *25*, 749–752. [CrossRef]
5. Elahi, H.; Munir, K.; Eugeni, M.; Atek, S.; Gaudenzi, P. Energy harvesting towards self-powered IoT devices. *Energies* **2020**, *13*, 5528. [CrossRef]
6. Costa, P.; Nunes-Pereira, J.; Pereira, N.; Castro, N. Sérgio Gonçalves, Senentxu Lanceros-Mendez, Recent progress on piezoelectric, pyroelectric, and magnetoelectric polymer-based energy-harvesting devices. *Energy Technol.* **2019**, *7*, 1800852. [CrossRef]
7. Khan, F.; Kowalchik, T.; Roundy, S.; Warren, R. Stretching-induced phase transitions in barium titanate-poly(vinylidene fluoride) flexible composite piezoelectric films. *Scr. Matr.* **2021**, *193*, 64–70. [CrossRef]
8. Marchiori, B.; Regal, S.; Arango, Y.; Delattre, R.; Blayac, S.; Ramuz, M. PVDF-TrFE-based stretchable contact and non-contact temperature sensor for e-skin Application. *Sensors* **2020**, *20*, 623. [CrossRef]
9. Tiwari, V.; Srivastava, G. Effect of thermal processing conditions on the structure and dielectric properties of PVDF films. *J. Polym. Res.* **2014**, *21*, 587. [CrossRef]
10. Martins, P.; Lopes, A.C.; Lanceros-Mendez, S. Electroactive phase of poly(vinylidene fluoride): Determination, processing and applications. *Prog. Polym. Sci.* **2014**, *39*, 683–706. [CrossRef]
11. Sukumaran, S.; Chatbouri, S.; Rouxel, D.; Tisserand, E.; Thiebaud, F.; Zineb, T.B. Recent advances in flexible PVDF based piezoelectric polymer devices for energy harvesting applications. *J. Intell. Mater. Syst. Struct.* **2021**, *32*, 746–780. [CrossRef]
12. Xia, W.; Zhang, Z. PVDF-based dielectric polymer and their applications in electronic materials. *IET Nanodielectr.* **2018**, *1*, 17–31. [CrossRef]
13. Zou, D.; Liu, S.; Zhang, C.; Hong, Y.; Zhang, G.; Yang, Z. Flexible and translucent PZT films enhanced by the compositionally graded heterostructure for human body monitoring. *Nano Energy.* **2021**, *85*, 105984. [CrossRef]
14. Wankhade, S.H.; Tiwari, S.; Gaur, A. Pralay Maiti, PVDF–PZT nanohybrid based nanogenerator for energy harvesting applications. *Energy Report* **2020**, *6*, 358–364. [CrossRef]
15. Sharma, S.K.; Gaur, H.; Kulkarni, M.; Patil, G.; Bhattacharya, B.; Sharma, A. PZT–PDMS composite for active damping of vibrations, Compos. *Sci. Technol.* **2013**, *77*, 42–51.
16. Xu, L.; Xu, Y. Effect of Zr^{4+} content on crystal structure, micromorphology, ferroelectric and dielectric properties of $Ba(Zr_xTi_{1-x})O_3$ ceramics. *J. Mater. Sci. Mater. Electron.* **2020**, *31*, 5492–5498. [CrossRef]
17. Sharma, S.; Sharma, H.; Kumar, S.; Thakur, S.; Kotnala, R.K.; Negi, N.S. Analysis of sintering temperature effects on structural, dielectric, ferroelectric, and piezoelectric properties of BaZr0.2Ti0.8O3 ceramics prepared by sol–gel method. *J. Mater. Sci. Mater. Electron.* **2020**, *31*, 19168–19179. [CrossRef]
18. Badapanda, T.; Senthil, V.; Anwar, S.; Cavalcante, L.S.; Batista, N.C.; Longo, E. Structural and dielectric properties of polyvinyl alcohol/barium zirconium titanate polymere ceramic composite. *Curr. Appl. Phys.* **2013**, *13*, 1490–1495. [CrossRef]
19. Shin, D.J.; Ji, J.H.; Kim, J.; Jo, G.H.; Jeong, S.J.; Koh, J.H. Enhanced flexible piezoelectric energy harvesters based on $BaZrTiO_3$-$BaCaTiO_3$ nanoparticles/PVDF composite films with Cu floating electrodes. *J. Alloys Compd.* **2019**, *802*, 562–572. [CrossRef]
20. Dash, S.; Thakur, V.N.; Kumar, A.; Mahaling, R.N.; Patel, S.; Thomas, R.; Sahoo, B.; Pradhan, D.K. Enhancing functional properties of PVDF-HFP/BZT-BCT polymer-ceramic composites by surface hydroxylation of ceramic fillers. *Ceram. Int.* **2012**, *47*, 33563–33576. [CrossRef]
21. Mitharwal, C.; Geetanjali; Malhotra, S.; Bagla, A.; Srivastava, M.K.; Gupta, S.M.; Singh Negia, C.M.; Kara, E.; Kulkarnid, A.R.; Mitra, S. Performance of dopamine modified $0.5(Ba_{0.7}Ca_{0.3})TiO_3$-$0.5Ba(Zr_{0.2}Ti_{0.8})O_3$ filler in PVDF nanocomposite as flexible energy storage and harvester. *J. Alloys Compd.* **2021**, *876*, 160141. [CrossRef]
22. Vijatovic Petrovica, M.; Cordero, F.; Mercadelli, E.; Brunengo, E.; Ilic, N.; Galassi, C.; Despotovic, Z.; Bobic, J.; Dzunuzovic, A.; Stagnaro, P.; et al. Flexible lead-free NBT-BT/PVDF composite films by hot pressing for low- energy harvesting and storage. *J. Alloys Compd.* **2021**, *884*, 161071. [CrossRef]
23. Leung, C.M.; Chen, X.; Wang, T.; Tang, Y.; Duan, Z.; Zhao, X.; Zhou, H.; Wang, F. Enhanced Electromechanical Response in PVDF-BNBT Composite Nanofibers for Flexible Sensor Applications. *Materials* **2022**, *15*, 1769. [CrossRef] [PubMed]
24. Craciun, F.; Cordero, F.; Mercadelli, E.; Ilic, N.; Galassi, C.; Baldisserri, C.; Bobic, J.; Stagnaro, P.; Canu, G.; Buscaglia, M.T.; et al. Flexible composite films with enhanced piezoelectric properties for energy harvesting and wireless ultrasound-powered technology. *Compos. Part B Eng.* **2023**, *263*, 110835. [CrossRef]
25. Bobić, J.D.; Teixeira, G.F.; Grigalaitis, R.; Gyergyek, S.; Petrović, M.M.V.; Zaghete, M.A.; Stojanovic, B.D. PZT-NZF/CF ferrites flexible thick films: Structural, dielectric, ferroelectric and magnetic characterization. *J. Adv. Ceram.* **2019**, *8*, 545–554. [CrossRef]

26. Cai, X.; Lei, T.; Sun, D.; Lin, L. A critical analysis of the α, β and γ phases in poly(vinylidene fluoride) using FTIR. *RSC Adv.* **2017**, *7*, 15382. [CrossRef]
27. Mahato, P.K.; Seal, A.; Garain, S.; Sen, S. Effect of fabrication technique on the crystalline phase and electrical properties of PVDF films. *Mater. Sci. Poland.* **2015**, *33*, 157–162. [CrossRef]
28. Makadeva, S.; Berring, J.; Walus, K.; Stoeber, B. Effect of poling time and grid voltage on phase transition and piezoelectricity of poly(vinyedene fluoride) thin films using corona poling. *J. Phys. D Appl. Phys.* **2013**, *46*, 285305. [CrossRef]
29. Lutterotti, L. Total pattern fitting for the combined size-strain-stress-texture determination in thin film diffraction. *Nucl. Instrum. Meth. Phys. Res. B* **2010**, *268*, 334–340. [CrossRef]
30. Karapuzha, A.S.; James, N.K.; Khanbareh, H.; Zwaag, S.; Groen, W.A. Structure, dielectric and piezoelectric properties of donor doped PZT ceramics across the phase diagram. *Ferroelectrics* **2016**, *504*, 160–171. [CrossRef]
31. Soo, M.; Mi, X.; Goroshin, S.; Higginsa, A.J.; Bergthorson, J.M. Combustion of particles, agglomerates, and suspensions—A basic thermophysical analysis. *Combust. Flame* **2018**, *192*, 384–400. [CrossRef]
32. Shepelin, N.A.; Glushenkov, A.M.; Lussini, V.C.; Fox, P.J.; Dicinoski, G.W.; Shapter, J.G.; Ellis, A.V. New developments in composites, copolymer technologies and processing techniques for flexible fluoropolymer piezoelectric generators for efficient energy harvesting. *Energy Environ. Sci.* **2019**, *12*, 1143–1176. [CrossRef]
33. Dash, S.; Mohanty, H.S.; Chauhan, R.; Kumar, A.; Thomas, R.; Pradhan, D.K. Ferroelectric ceramic dispersion to enhance the β phase of polymer for improving dielectric and ferroelectric properties of the composites. *Polym. Bull.* **2021**, *78*, 5317–5336. [CrossRef]
34. Seena, M.; Jan, H.; Prasad, V. Dielectric properties of hot-pressed Poly(vinylidene fluoride)/Functionalized carbon nanotube composites. *Mater. Chem. Phys.* **2022**, *285*, 126134. [CrossRef]
35. Huang, Z.X.; Wang, M.M.; Feng, Y.H.; Qu, J.P. β-Phase Formation of Polyvinylidene Fluoride via Hot Pressing under Cyclic Pulsating Pressure. *Macromolecules* **2020**, *53*, 8494–8501. [CrossRef]
36. Muduli, S.P.; Parida, S.; Rout, S.K.; Rajput, S.; Kar, M. Effect of hot press temperature on β-phase, dielectric and ferroelectric properties of solvent casted Poly(vinyledene fluoride) films. *Mater. Res. Express* **2016**, *6*, 095306. [CrossRef]
37. Yang, D.; Chen, Y. β-phase formation of poly(vinylidene fluoride) from the melt induced by quenching. *J. Mater. Sci. Lett.* **1987**, *6*, 599−603. [CrossRef]
38. Mohanty, H.S.; Chauhan, R.; Kumar, A.; Kulriya, P.K.; Thomasd, R.; Pradhan, D.K. Dielectric/ferroelectric properties of ferroelectric ceramic dispersed poly (vinylidene fluoride) with enhanced β-phase formation. *Mater. Chem. Phys.* **2019**, *230*, 221–230. [CrossRef]
39. Balaraman, A.A.; Dutta, S. Inorganic dielectric materials for energy storage applications: A review. *J. Phys. D Appl. Phys.* **2022**, *55*, 183002. [CrossRef]
40. Jain, A.; Prashanth, K.J.; Sharma, A.K.; Jain, A.; Rashmi, P.N. Dielectric and Piezoelectric Properties of PVDF/PZT Composites: A Review, Published online in Wiley Online Library. *Polym. Eng. Sci.* **2015**, *55*, 1589–1616. [CrossRef]
41. Sun, E.; Cao, W. Relaxor-based ferroelectric single crystals: Growth, domain engineering, characterization and applications. *Prog. Mater. Sci.* **2014**, *65*, 124–210. [CrossRef]
42. Brunengo, E.; Conzatti, L.; Schizzi, I.; Buscaglia, M.T.; Canu, G.; Curecheriu, L.; Costa, C.; Castellano, M.; Mitoseriu, L.; Stagnaro, P.; et al. Improved dielectric properties of poly(vinylidene fluoride)–$BaTiO_3$ composites by solvent-free processing. *J. Appl. Polym. Sci.* **2021**, *138*, e50049. [CrossRef]
43. Samet, M.; Kallel, A.; Serghei, A. Maxwell-Wagner-Sillars interfacial polarization in dielectric spectra of composite materials: Scaling laws and applications. *J. Compos. Mater.* **2022**, *56*, 3197–3217. [CrossRef]
44. Yang, L.; Kong, X.; Cheng, Z.; Zhang, S. Ultra-high energy storage performance with mitigated polarization saturation in lead-free relaxors. *J. Mater. Chem. A* **2019**, *7*, 8573. [CrossRef]
45. Mishra, K.K.; Instan, A.A.; Kumari, S.; Scott, J.F.; Katiyar, R.S. Lead palladium titanate: A room temperature nanoscale multiferroic thin film. *Sci. Rep.* **2020**, *10*, 2991. [CrossRef] [PubMed]
46. Fletcher, N.H.; Hilton, A.D.; Ricketts, B.W. Optimization of energy storage density in ceramic capacitors. *J. Phys. D Appl. Phys.* **1996**, *29*, 253. [CrossRef]
47. Hou, Y.; Deng, Y.; Wang, Y.; Gao, H. Uniform distribution of low content $BaTiO_3$ nanoparticles in poly(vinylidene fluoride) nanocomposite: Toward high dielectric breakdown strength and energy storage density. *RSC Adv.* **2015**, *5*, 72090. [CrossRef]
48. Chi, Q.; Liu, G.; Zhang, C.; Cui, Y.; Wang, X.; Lei, Q. Microstructure and dielectric properties of BZT-BCT/PVDF nanocomposites. *Results Phys.* **2018**, *8*, 391–396. [CrossRef]
49. Mei, W.; Wei, J.; Ko, Z.Y.; Cheng, Z.Y.; Hu, J. Novel P(VDF-HFP)/BST nanocomposite films with enhanced dielectric properties and optimized energy storage performance. *Ceram. Int.* **2021**, *47*, 15561–15567. [CrossRef]
50. Liu, S.; Xue, S.; Xiu, S.; Shen, B.; Zhai, J. Surface-modified $Ba(Zr_{0.3}Ti_{0.7})O_3$ nanofibers by polyvinylpyrrolidone filler for poly(vinylidene fluoride) composites with enhanced dielectric constant and energy storage density. *Sci. Rep. UK* **2016**, *6*, 26198. [CrossRef]
51. Luo, H.; Zhou, X.; Ellingford, C.; Zhang, Y.; Chen, S.; Zhou, K.; Zhang, D.; Bowen, C.R. Chaoying Wan, Interface design for high energy density polymer nanocomposites. *Chem. Soc. Rev.* **2019**, *48*, 4424. [CrossRef]

52. Wang, Y.; Wang, H.; Xu, K.; Wang, B.; Wang, F.; Li, C.; Diao, C.; Huang, H.; Zheng, H. Significantly improved energy storage performance of flexible PVDF-based nanocomposite by loading surface-hydroxylated $BaZr_{0.2}Ti_{0.8}O_3$ nanofibers. *Ceram. Int.* **2022**, *48*, 16114–16122. [CrossRef]
53. Hao, X. A review on the dielectric materials for high energy-storage application. *J. Adv. Dielect.* **2013**, *3*, 1330001. [CrossRef]
54. Jeder, K.; Bouhamed, A.; Nouri, H.; Abdelmoula, N.; Johrmann, N.; Wunderle, B.; Khemakhem, H.; Kanoun, O. Enhancement of the performance of flexible lead-free nanogenerators by doping in $BaTiO_3$ nanoparticles. *Energy* **2022**, *261*, 125169. [CrossRef]
55. Liu, J.; Yang, B.; Liu, J. Development of environmental-friendly BZT–BCT/P(VDF–TrFE) composite film for piezoelectric generator. *J. Mater. Sci. Mater. Electron.* **2018**, *29*, 17764–17770. [CrossRef]
56. Liu, J.; Yang, B.; Lu, L.; Wang, X.; Li, X.; Chen, X.; Liu, J. Flexible and lead-free piezoelectric nanogenerator as self-poweredsensor based on electrospinning BZT-BCT/P(VDF-TrFE) nanofibers. *Sens. Actuat. A-Phys.* **2020**, *303*, 111796. [CrossRef]